presence of exogenous hypoxanthine, adenine, or their respective nucleosides.

In conclusion, CBV is a new anti-HIV compound endowed with selective and potent antiretrovial activity. Our current studies suggest strongly the strategy of exploring the effect of nucleobases, nucleosides, or other compounds to enhance the antiretroviral effectiveness of CBV.

ACKNOWLEDGMENTS

We thank Michele Connelly for her technical assistance and Dolores Anderson for her patient typing of the manuscript.

REFERENCES

Ahluwalia, G., Cooney, D. A., Mitsuya, H., Fridland, A., Flora, K. P., Hao, Z., Dalal, M., Broder, S., & Johns, D. G. (1987) *Biochem. Biophys. Res. Commun. 36*, 3797–3800.

Balzarini, J. R., Pauwels, R., Herdewijn, P., DeClercq, E., Cooney, D. A., Kong, C. J., Dulal, M., Johns, D. G., & Broder, S. (1987) *Biochem. Biophys. Res. Commun. 140*, 735–742.

Bestwick, R. K., Moffett, G. L., & Mathews, C. K. (1982) *J. Biol. Chem. 257*, 9300–9304.

Johnson, M., & Fridland, A. (1989) *Mol. Pharmacol. 36*, 291–295.

Johnson, M. A., Ahluwalia, G., Connelly, M. C., Cooney, D. A., Broder, S., Johns, D. G., & Fridland, A. (1988) *J. Biol. Chem. 263*, 15354–15357.

Mitsuya, H., & Broder, S. (1986) *Proc. Natl. Acad. Sci. U.S.A. 83*, 1911–1915.

Richman, D. D., Fischl, M. A., Grieco, M. H., Gottlieb, M. S., Volberding, P. A., Laskin, O. L., Leedom, J. M., Groopman, G. E., Mildvan, D., Hirsch, M. S., Jackson, G. G., Durack, D. T., Phil, D., & Nusinoff-Lehrman, S. (1987) *N. Engl. J. Med. 317*, 192–197.

Sarup, J. C., & Fridland, A. (1987) *Biochemistry 26*, 590–597.

Srere, P. A. (1969) *Methods Enzymol. 13*, 3–11.

Verhoef, V., Sarup, J., & Fridland, A. (1981) *Cancer Res. 41*, 4478–4483.

Vince, R., & Hua, M. (1990) *J. Med. Chem. 33*, 17–21.

Vince, R., Hua, M., Brownell, J., Daluge, S., Lee, F., Shannon, W. M., Lavelle, G. C., Qualls, J., Weislow, O. S., Kiser, R., Canonico, P. G., Schultz, R. H., Narayanan, V. L., Mayo, J. G., Shoemaker, R. H., & Boyd, M. R. (1988) *Biochem. Biophys. Res. Commun. 156*, 1046–1053.

White, E. L., Parker, W. b., Macy, L. J., Shaddix, S. C., McCaleb, G, Secrist, J. A., III, Vince, R., & Shannon, W. M. (1989) *Biochem. Biophys. Res. Commun. 161*, 393–398.

Yarchoan, r., Perno, C. F., Thomas, R. V., Klecker, R. W., Allain, J. P., Wills, R. J., McAtt, N., Fischl, M. A., Dubinsky, R., McNeely, M. C., Mitsuya, H., Pluda, J. M., Lawley, T. J., Leuther, M., Safai, B., Collins, J. M., Myers, C. E., & Broder, S. (1988) *Lancet i*, 76–81.

# NMR and Computational Studies of Interactions between Remote Residues in Gangliosides†

J. Neel Scarsdale,*,‡ James H. Prestegard,§ and Robert K. Yu‡

*Department of Biochemistry and Molecular Biophysics, Virginia Commonwealth University, Box 614 MCV Station, Richmond, Virginia 23298-0614, and Department of Chemistry, Yale University, Box 6666 Yale Station, New Haven, Connecticut 06511*

*Received March 21, 1990; Revised Manuscript Received July 27, 1990*

ABSTRACT: Conformational preferences of the gangliosides GM1, GM1b, and GD1a have been investigated by using a systematic combination of NMR distance constraints and molecular mechanics calculations. These gangliosides share a common four-sugar core but differ in the number or placement of sialic acid residues attached to the core. Placement of the sialic acid residues is shown to influence the preferred core conformation. The origin of these effects is postulated to be intramolecular interactions of the sialic acid residues with other remote residues. In the case of GM1, hydrogen bonds between the internal sialic acid and an *N*-acetyl group on GalNAc are suggested. In the case of GD1a, a hydrogen-bonding network between the terminal and internal sialic acids is suggested to play a role.

Cell surface oligosaccharides, such as those which occur in the headgroups of glycolipids, display a diversity in both primary structure and tertiary conformation that makes them useful mediators of cell-specific interactions. Although there is general recognition of the importance of sequence-specific recognition of these cell surface receptors, there have been few attempts to delineate direct recognition of residue functionality from recognition of conformational properties of specific regions. It is not always easy to distinguish between these possibilities because alteration of primary structure at a point well removed from the oligosaccharide segment involved in recognition may in principle affect the conformation of the recognition site. Only recently has evidence begun to accumulate to suggest the importance of conformation and modulation of this conformation by remote residue substitution.

Biochemical data on the specificity of some closely related antibodies can be interpreted in terms of remote group induced alterations in the conformation of primary recognition sites. One example occurs in the case of type-specific streptococcal polysaccharides (Jennings & Kasper, 1981; Schifferle et al., 1985). Antisera raised against type III group B streptococci were determined to contain two antigenically distinct populations of antibodies (Kasper et al., 1979; Jennings et al., 1980). One class of antibodies is specific for the native type III antigen, which has a $\beta$1→4Glc($\beta$1–4)[NeuAc($\alpha$2–6)]Gal($\beta$1–4)GlcNAc($\beta$1–4)Gal repeating unit, while a second class of

† This research was supported by USPHS Grants GM33225 (J.H.P.) and NS11853 (R.K.Y.).

* Author to whom correspondence should be addressed.
‡ Virginia Commonwealth University.
§ Yale University.

0006-2960/90/0429-9843$02.50/0 

antibodies is specific for the core antigen, which has a $\beta 1\rightarrow$-4Glc($\beta$1-4)Gal($\beta$1-4)GlcNAc($\beta$1-4)Gal repeating unit. Further studies (Jennings & Kasper, 1981) have indicated that reduction of the $COO^-$ group of the $\alpha$-D-NeuAc residues in the native polysaccharide destroys the antigenicity of this polysaccharide against antibodies specific for the native polysaccharide. On the other hand, the antigenicity of this oligosaccharide against antibodies specific for the native antigen was unaffected by sterically larger changes such as the removal of both C8 and C9 from the glyceryl side chains of the $\alpha$-D-NeuAc residues of the native antigen. Furthermore, both the reduced native polysaccharide and the core polysaccharide showed equal reactivities with antibodies directed against the core antigen. Together, these results suggest that the $\alpha$-D-NeuAc residues may not be an integral part of the immunological determinant of the native antigen, but rather the $COO^-$ group may be involved in interactions which influence the conformation of the core oligosaccharide determinant (Jennings & Kasper, 1981). The $COO^-$ group of sialic acid is a rather strong hydrogen bond acceptor and in the native type III antigen could easily be involved in hydrogen-bonding interactions which influence the conformation of the Gal($\beta$1-4)GlcNAc linkage (Jennings & Kasper, 1981).

There is also direct physical evidence supporting remote group induced changes in oligosaccharide conformation. The possibility of such interactions was suggested on the basis of significant perturbations in the chemical shifts of $^1H$ resonances corresponding to protons on the $\beta$-D-GalNAc residues of gangliosides GM1[1] and GM2, which were absent in their asialo derivatives (Koerner et al., 1983). Some additional examples of long-range effects have recently been reported in studies of the solution conformation of several related multiantennary N-linked oligosaccharides from glycoproteins (Homans et al., 1986). In the case of these oligosaccharides, it was noted that the orientation of the Man($\alpha$1-6)Man($\beta$1-) arm, as reflected in the values of the vicinal coupling constants for the $\beta$-D-mannose H6 protons, apparently depended on interactions involving residues that were far removed in the primary sequence from the Man($\alpha$1-6)Man linkage.

There is not, however, universal agreement on the importance of these effects. Earlier studies of the solution conformation of gangliosides GM1, GM2, and their asialo derivatives (Sabesean et al., 1984) based on a combination of one-dimensional equilibrium NOE measurements and Bock and Lemieux's HSEA algorithm (Lemieux et al., 1980; Thørgeson et al., 1982) found no evidence for structural perturbations resulting from interactions involving $\alpha$-D-NeuAc residues. The minimally parametrized potential surface used in these early studies, however, neglects contributions from energy terms such as hydrogen-bonding and electrostatic interactions which could be important in through-space interactions involving the highly charged $\alpha$-D-NeuAc residues. Molecular mechanics calculations, on the other hand, use a more elaborately parametrized force field that includes electrostatic and hydrogen-bonding interactions. Although some additional work on related sialic acid containing molecules has appeared recently (Bregg et al., 1989), a reinvestigation of ganglioside solution conformation would seem to be in order.

[1] Abbreviations: DMSO, dimethyl sulfoxide; $D_2O$, deuterated water; GM1, Gal($\beta$1-3)GalNAc($\beta$1-4[NeuAc($\alpha$2-3)]Gal($\beta$1-4)Glc($\beta$1-1')-Cer; GM1b, NeuAc($\alpha$2-3)Gal($\beta$1-3)GalNAc($\beta$1-4)Gal($\beta$1-4)Glc($\beta$1-1')Cer; GM2, GalNAc($\beta$1-4)[NeuAc($\alpha$2-3)]Gal($\beta$1-4)Glc($\beta$1-1')Cer; GD1a, NeuAc($\alpha$2-3)Gal($\beta$1-3)GalNAc($\beta$1-4)[NeuAc($\alpha$2-3)]Gal($\beta$1-4)Glc($\beta$1-1')Cer; NMR, nuclear magnetic resonance; NOE, nuclear Overhauser effect; ppm, parts per million; RMS, root mean square.

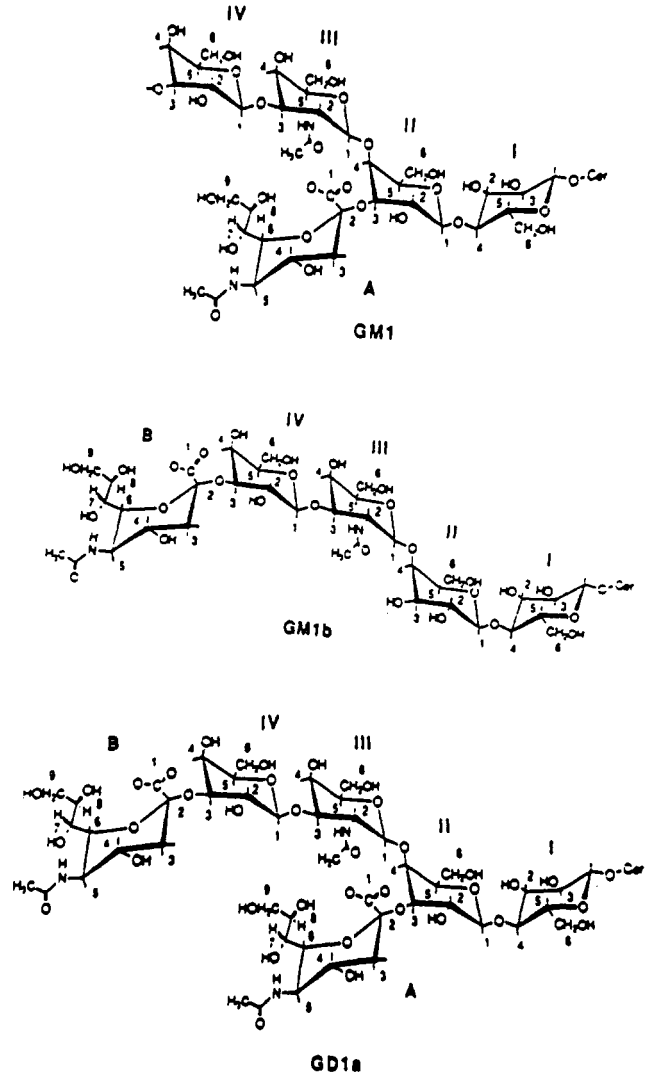


FIGURE 1: Primary structures of gangliosides GM1, GM1b, and GD1a.

Here, we shall use a combination of NMR distance constraints, treated as pseudoenergies (Holak et al., 1987; Scarsdale et al., 1988), and molecular mechanics calculations to investigate the influence of through-space interactions involving specific pairs of saccharide residues on the solution conformation of gangliosides GM1, GM1b, and GD1a in DMSO-$d_6$/$D_2O$ (98:2 v/v). The primary structures for these gangliosides are shown in Figure 1. These gangliosides all share the same Gal($\beta$1-3)GalNAc($\beta$1-4)Gal($\beta$1-4)Glc core oligosaccharide sequence and differ from one another in the number of $\alpha$-D-NeuAc residues as well as in the linkage sites for these residues. We shall investigate the influence of through-space interactions on the solution conformation of these gangliosides by comparing the three-dimensional structure of oligosaccharide sequences common to these gangliosides.

## Experimental Methodology

Gangliosides GM1 and GD1a and GM1b were isolated in our laboratories as described previously (Ando & Yu, 1977; Ariga & Yu 1987). Samples of the sodium salts of each of these gangliosides were dissolved in DMSO-$d_6$/$D_2O$ (98:2 v/v), a medium chosen to optimize solubility and minimize micelle formation. Although this is unlikely to reproduce the membrane surface environment in which these molecules function as receptors, it is not clear that removal of the hydrophobic lipid portion of the molecule, so that the headgroup could be

Table I: $^1$H Resonance Assignments for Gangliosides GM1, GM1b, and GD1a

| compd | 1 | 2 | 3 | 4 | 5 | 6 | 7 | 8 | 9 |
|---|---|---|---|---|---|---|---|---|---|
| GM1[a] | | | | | | | | | |
| I | 4.15 | 3.03 | 3.34 | 3.28 | 3.29 | 3.63(a)<br>3.74(b) | | | |
| II | 4.28 | 3.13 | 3.73 | 3.92 | 3.49 | 3.47(a)<br>3.74(b) | | | |
| III | 4.86 | 3.91 | 3.47 | 3.72 | 3.63 | 3.37(a)<br>3.47(b) | | | |
| IV | 4.21 | 3.37 | 3.31 | 3.61 | 3.37 | 3.41(a)<br>3.74(b) | | | |
| A | | | 1.61(a)<br>2.53(e) | 3.71 | 3.36 | 3.11 | 3.17 | 3.49 | 3.36(a)<br>3.62(b) |
| GM1b | | | | | | | | | |
| I | 4.16 | 3.03 | 3.33 | 3.27 | 3.29 | 3.60(a)<br>3.75(b) | | | |
| II | 4.19 | 3.22 | 3.39 | 3.77 | 3.46 | | | | |
| III | 4.52 | 3.75 | 3.71 | 3.81 | 3.33 | | | | |
| IV | 4.24 | 3.27 | 3.91 | 3.69 | 3.20 | | | | |
| B | | | 1.35(a)<br>2.76(e) | 3.53 | 3.34 | 3.60 | 3.24 | 3.61 | 3.37(a)<br>3.46(b) |
| GD1a | | | | | | | | | |
| I | 4.14 | 3.03 | 3.33 | 3.28 | 3.26 | 3.60(a)<br>3.72(b) | | | |
| II | 4.28 | 3.21 | 3.82 | 3.92 | 3.46 | | | | |
| III | 4.78 | 3.93 | 3.54 | 3.73 | 3.65 | | | | |
| IV | 4.27 | 3.25 | 3.94 | 3.75 | 3.27 | | | | |
| A | | | 1.61(a)<br>2.61(e) | 3.67 | 3.37 | 3.16 | 3.19 | 3.49 | 3.33(a)<br>3.60(b) |
| B | | | 1.35(a)<br>2.76(e) | 3.55 | 3.40 | 3.33 | 3.27 | 3.49 | 3.37(a)<br>3.49(b) |

[a] Assignments taken from Koerner et al. (1983).

dissolved in an aqueous environment, would produce a more realistic model for study. In Table I, we present $^1$H resonance assignments for each of the compounds in Figure 1. These assignments were made by using a combination of two-dimensional homonuclear proton scalar coupling correlated experiments and two-dimensional cross-relaxation correlated experiments as reported previously (Scarsdale et al., 1986a).

From the data in Table I, a number of facts are worth noting. In gangliosides GM1 and GD1a, the presence of an internally linked α-D-NeuAc residue results in significant downfield shifts for the H1 and H2 resonances of β-D-GalNAc III. These downfield shifts are absent in ganglioside GM1b, which lacks an internally linked α-D-NeuAc residue. Furthermore, the chemical shifts for the H3a and H3e protons of the internally linked α-D-NeuAc residue in gangliosides GM1 and GD1a differ significantly from the chemical shifts for these protons for the terminally linked α-D-NeuAc residue in gangliosides GM1b and GD1a. These chemical shift perturbations are likely the result of through-space interactions between the internal α-D-NeuAc residue which is linked to C3 of β-D-Gal II and the β-D-GalNAc residue which is linked to C4 of the same residue in gangliosides GM1 and GD1a. It is easy to imagine that this pair of saccharide residues can be spatially proximate and therefore capable of influencing the local magnetic field experienced by protons on one or the other.

Chemical shift changes, however, can arise through a variety of mechanisms and interpretation in terms of a specific conformational basis is at best risky. Therefore, to provide a sound structural description for these postulated through-space interactions, we have performed two-dimensional cross-relaxation correlated experiments on gangliosides GM1, GM1b, and GD1a dissolved in DMSO-$d_6$/$D_2O$.

Since the experimental and calculational methodologies used in the determination of the solution conformation of each of these gangliosides were virtually identical, we shall illustrate the methodologies using ganglioside GD1a. This ganglioside is the most complex glycolipid in this study and thus should serve to illustrate many of the problems associated with the structure determination of these gangliosides.

A two-dimensional pure absorption cross-relaxation correlated experiment was acquired with a mixing time of 250 ms on a sample (2 mg) of ganglioside GD1a dissolved in DMSO-$d_6$/$D_2O$ (98:2 v/v). This mixing time represents a reasonable compromise between the often conflicting demands that the mixing times be short enough so that a simple inverse sixth power relationship between cross-peak intensity and internuclear distance is valid but that the mixing times be long enough to provide an adequate signal to noise ratio. Previous studies (Scarsdale et al., 1986b) on a glycolipid of similar size with the same mixing time have yielded internuclear distances that were in reasonable agreement with those determined on the basis of a more complete analysis of the time-dependent evolution of cross-peak intensities in two-dimensional data sets or on the basis of one-dimensional NOE measurements.

In Figure 2, we present a contour plot of the region of this NOESY experiment that contains connectivities between all of the oligosaccharide protons, save those which involve the geminal three proton resonances of the two α-D-NeuAc residues. In Figure 2, we also present a contour plot of the region containing connectivities involving the geminal H3a and H3e resonances from the two α-D-NeuAc residues. This NOESY experiment was obtained at 303 K on a Bruker WM500 spectrometer. This data set consisted of 192 real and 192 imaginary $t_1$ points which were acquired and stored separately to achieve quadrature in the $t_1$ dimension (States et al., 1982). Each $t_1$ point consisted of 1K complex points over a 3205-Hz sweep width averaged for 64 transients with a 1.2-s repetition rate. Data were processed for phase-sensitive display with the FTNMR program[2] using cosine bell weighting functions and zero

[2] FTNMR is obtained via a licensing agreement with Hare Research, Inc.

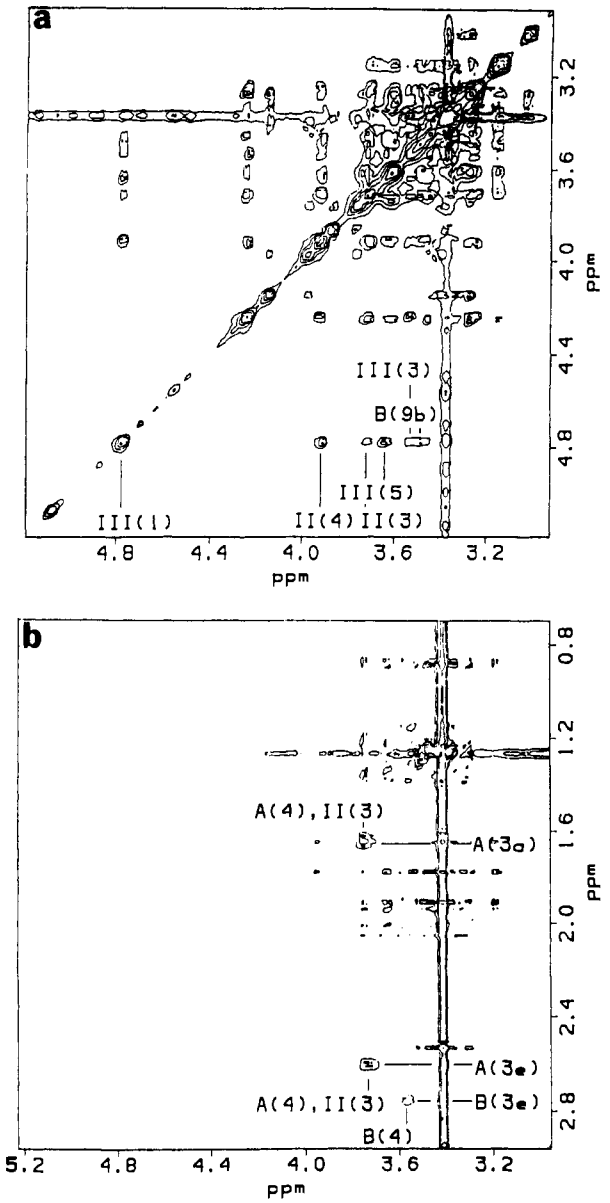


FIGURE 2: Contour plots of regions from a 250-ms NOESY data set for GD1a. (a) Connectivities between all oligosaccharide protons save those involving the geminal H3 protons of α-D-NeuAc residues A and B. (b) Connectivities between core oligosaccharide protons and geminal H3 protons of α-D-NeuAc residues A and B.

filling in both dimensions to yield a 2K × 2K data matrix.

From the data in Figure 2, a number of facts are worth noting. In addition to the expected intraresidue connectivities to the H3 and H5 protons, each anomeric resonance possesses two or more interresidue connectivities. For instance, the resonance at 4.78 ppm, which is assigned to the anomeric resonance of β-D-GalNAc III, shows intraresidue connectivities to the III(3) and III(5) resonances at 3.54 and 3.65 ppm, respectively, and interresidue connectivities to the II(3) and II(4) resonances at 3.82 and 3.92 ppm, respectively. In all cases, the strongest interresidue cross-peak corresponds to the aglyconic proton resonance.

A particularly interesting connectivity is the connectivity from the anomeric resonance of β-D-GalNac III to a resonance at 3.49 ppm. Examination of the assignment data in Table I reveals that the II(5) resonance is the only resonance from either sequentially adjacent residue which is near 3.49 ppm. If we assume that the cross-relaxation data are to be interpreted in terms of a single rigid conformer, the fact that the connectivity is observed to the II(3) resonance makes it impossible for the anomeric proton of β-D-GalNAc III to be simultaneously spatially proximate to the II(5) proton. If we neglect the possibility that this connectivity results from an unassigned H6a or H6b resonance, which is unlikely given the connectivity to the II(3) resonance, we must conclude that the connectivity to a resonance at 3.49 ppm results from a proton which is spatially proximate but sequentially remote to the III(1) proton. Further examination of the assignment data in Table I reveals that the A(8), B(8), and B(9b) protons all have resonances near 3.49 ppm. Of these three possibilities, only the B(8) and B(9b) protons can be spatially proximate to the III(1) proton, given the constraints imposed by the primary structure of ganglioside GD1a and the fact that the A(9b) proton is also spatially proximate to the IV(1) proton.

To establish a preference for one of these remaining possibilities, we have chosen to carry out molecular mechanics calculations with NMR distance constraints (Scarsdale et al., 1988) for each of the two possibilities. The calculations in which the B(9b) proton was constrained to be spatially proximate to the III(1) proton led to structures with significantly lower energies, which led us to conclude that the connectivitiy to a resonance near 3.49 ppm is due to the B(9b) proton.

Internuclear distance constraints can be obtained from a simple ratio of cross-peak volumes in pure absorption NOESY experiments provided these cross-peaks can be interpreted as arising from relaxation in a rigid, nearly isotropically tumbling, molecule. Cross-peak volumes were obtained by using the method of Holak et al. (1987a) in which the cross-peak volume is the product of the integrals of a row and column through the cross-peak divided by the intensity at the intersection of the row and column. Cross-peak volumes were converted to distance constraints through the use of an expression of the form

$$r_{ij} = (a_0/a_{ij})^{1/6} r_0 \quad (1)$$

In eq 1, $r_{ij}$ is the distance between a given pair of protons, and $a_{ij}$ is the corresponding cross-peak volume; $a_0$ is the cross-peak volume corresponding to a pair of a protons to be used as a calibration standard, and $r_0$ is the corresponding distance.

In most naturally occurring gangliosides, the saccharide residues are believed to be rigidly fixed in a chair conformation. Hence, there are a number of intraresidue proton pairs that serve as calibration standards beween internuclear distance and cross-peak intensity. In the case of β-D-glucosides and β-D-galactosides, these standards are provided by the H1–H3, H1–H5, and H3–H5 cross-peaks, all at a distance of approximately 2.5 Å. For β-D-galactosides, additional standards were provided by the H3–H4 and H4–H5 cross-peaks, also at 2.5 Å. In the case of the α-D-NeuAc residues, these standards were provided by the H3e–H4, H3a–H5, and H4–H6 cross peaks, all at a distance of 2.5 Å.

Error limits for distance constraints are obtained by propagating statistical errors observed by measuring peak volumes for several different row and column combinations. For a cross-peak corresponding to a 3.0-Å separation, these volume errors were typically on the order of 40%. These volume errors were converted to upper and lower bounds for the corresponding distances through the use of eq 1, which for a 3.0-Å constraint were typically 3.3 and 2.8 Å, respectively. In Table II, we present a list of distance constraints and corresponding error limits obtained from NOESY data sets for each of the compounds in Figure 1.

Examination of the data in Table II reveals that there are no connectivities between protons on α-D-NeuAc A and β-D-GalNAc III in either ganglioside GM1 or GD1a. In other

Table II: Distance Constraints and Associated Errors for Gangliosides GM1, GM1b, and GD1a

| | GM1 | GM1b | GD1a |
|---|---|---|---|
| II(1)–II(3)[a] | 2.5 (–0.1) (+0.0) | 2.5 (–0.1) (+0.1) | 2.5 (–0.1) (+0.1) |
| II(1)–II(5)[a] | 2.5 (–0.1) (+0.0) | 2.5 (–0.1) (+0.1) | 2.5 (–0.1) (+0.1) |
| II(1)–I(4) | 2.2 (–0.0) (+0.0) | 2.1 (–0.0) (+0.0) | 2.2 (–0.0) (+0.1) |
| II(1)–I(6a) | 3.3 (–0.2) (+0.4) | 3.3 (–0.3) (+0.7) | 2.9 (–0.2) (+0.2) |
| II(1)–I(6b) | ≥4.0 | 2.8 (–0.1) (+0.2) | 3.1 (–0.3) (+0.5) |
| III(1)–III(3)[a] | 2.5 (–0.1) (+0.0) | 2.5 (–0.1) (+0.1) | 2.5 (–0.1) (+0.1) |
| III(1)–III(5)[a] | 2.5 (–0.1) (+0.0) | 2.5 (–0.1) (+0.1) | 2.5 (–0.1) (+0.1) |
| III(1)–II(3) | 3.0 (–0.1) (+0.1) | ≥4.0 | 2.8 (–0.1) (+0.2) |
| III(1)–II(4) | 2.4 (–0.1) (+0.1) | 2.2 (–0.1) (+0.0) | 2.3 (–0.0) (+0.0) |
| III(1)–II(5) | ≥4.0 | 2.8 (–0.2) (+0.3) | ≥4.0 |
| IV(1)–IV(3)[a] | 2.5 (–0.0) (+0.1) | 2.6 (–0.1) (+0.1)[b] | 2.5 (–0.1) (+0.1) |
| IV(1)–IV(5)[a] | 2.5 (–0.0) (+0.1) | 2.3 (–0.1) (+0.1)[b] | 2.5 (–0.1) (+0.1) |
| IV(1)–III(3) | 2.5 (–0.1) (+0.1) | 2.2 (–0.1) (+0.0) | 2.4 (–0.0) (+0.1) |
| IV(1)–III(4) | 3.1 (–0.1) (+0.3) | 3.3 (–0.4) (+0.7) | 3.1 (–0.2) (+0.5) |
| A(3e)–A(4)[a] | 2.5 (–0.0) (+0.0) | | 2.5 (–0.0) (+0.1) |
| A(4)–A(6)[a] | 2.5 (–0.0) (+0.0) | | 2.5 (–0.0) (+0.1) |
| A(7)–A(9b) | | | 2.6 (–0.0) (+0.1) |
| A(3a)–II(3) | 2.3 (–0.0) (+0.0) | | 2.4 (–0.0) (+0.1) |
| A(3e)–II(3) | 2.7 (–0.0) (+0.1) | | 2.9 (–0.2) (+0.1) |
| A(3a)–II(4) | 3.4 (–0.3) (+0.4) | | 3.1 (–0.2) (+0.4) |
| A(3e)–II(4) | 3.2 (–0.2) (+0.3) | | ≥4.0 |
| A(9b)–IV(1) | 3.0 (–0.2) (+0.2) | | 3.1 (–0.2) (+0.5) |
| B(3e)–B(4)[a] | | 2.5 (–0.2) (+0.4) | 2.5 (–0.1) (+0.1) |
| B(3a)–IV(3) | | ≥4.0 | ≥4.0 |
| B(3e)–IV(3) | | 2.7 (–0.3) (+0.8) | ≥4.0 |
| B(9b)–III(1) | | ≥4.0 | 2.5 (–0.1) (+0.1) |

[a] Rigidly fixed intraresidue distance used as an intensity standard for calculating unknown interresidue distances. [b] Intraresidue distance calculated based on average over intensities for IV(1)–IV(3), IV(1)–IV(5), IV(3)–IV(4), and IV(4)–IV(5) crosspeaks. In the molecular mechanics calculation, these distances were set equal to 2.5 Å.

words, there is no evidence based on through-space connectivities that these two residues are spatially proximate in either of these gangliosides. The data, however, do reveal significant differences in the interresidue connectivities between β-D-GalNAc III and β-D-Gal II for gangliosides GM1 and GD1a, which possess an internally linked α-D-NeuAc residue, and ganglioside GM1b, which lacks this internally linked α-D-NeuAc residue. In gangliosides GM1 and GD1a, the III(1) proton is spatially proximate to both the II(4) aglyconic proton and the II(3) proton, while in ganglioside GM1b, the III(1) proton is spatially proximate to the II(4) and II(5) protons. These qualitative differences in interresidue connectivities are indicative of significant differences in the conformation of the GalNAc(β1–4)Gal (III,II) linkage in gangliosides GM1 and GD1a as compared to ganglioside GM1b.

Further examination of the data in Table II reveals significant differences in the connectivities for the terminal NeuAc(α2–3)Gal (B,IV) linkage between gangliosides GD1a and GM1b, which differ from one another only in that ganglioside GD1a has an additional internally linked α-D-NeuAc residue. In ganglioside GM1b, the B(3e) proton is spatially proximate to the IV(3) aglyconic proton, while in ganglioside GD1a, neither the B(3a) nor B(3e) proton is spatially proximate to the IV(3) aglyconic proton. In other words, the addition of an internally linked α-D-NeuAc residue in ganglioside GD1a resulted in significant perturbations of the conformation of the terminal NeuAc(α2–3)Gal linkage, as compared to ganglioside GM1b. Thus, it appears that conformational perturbations may involve residues which are proximate to one another in the primary sequence, as is the case with the internal α-D-NeuAc and β-D-GalNAc residues in gangliosides GM1 and GD1a, or residues which are quite distant from one another in the primary sequence, as is the case with the internal and terminal α-D-NeuAc residues in ganglioside GD1a.

## Calculational Methodology

To use the distance constraints listed in Table II in the calculation of a three-dimensional structure, we have chosen to use a combination of molecular mechanics calculations and distance constraint pseudoenergies (Scarsdale et al., 1988; Holak et al., 1987b). We use the molecular mechanics program from the AMBER[3] (Assisted Model Building with Energy Refinement) package (Weiner & Kollman, 1981) which we have modified to include a pseudoenergy function that more accurately reflects the inverse sixth power distance dependence of the NOE than the harmonic potential function typically used to represent distance constraints (Scarsdale et al., 1988; Holak et al., 1987b). In these calculations, the standard AMBER force field was modified as described previously (Scarsdale et al., 1988) to reflect bonding situations that are unique to glycoconjugates and to allow for the explicit specification of lone pair electrons on the glycosidic and ring oxygens on each residue.

When a simplified potential surface is used in the initial stages of the calculation, the use of NMR distance constraint peudoenergies has proven useful in avoiding some of the local minimum traps which have often plagued molecular mechanics calculations (Holak et al., 1987b; Scarsdale et al., 1988). To further ensure the location of global minimum energy structures as opposed to local minimum energy structures, we also use several starting structures that are well displaced from one another in conformational space. These structures differ from one another in terms of the orientations of their saccharide residues as defined by the glycosidic torsion angles $\phi$ and $\psi$. For β-D-glucosides and β-D-galactosides, $\phi$ is the dihedral angle defined by the anomeric proton, the anomeric carbon, the glycosidic oxygen, and the aglyconic carbon, and $\psi$ is the dihedral angle defined by the anomeric carbon, the glycosic oxygen, the aglyconic carbon, and the aglyconic proton. For α-D-NeuAc residues, which lack an anomeric proton, $\phi$ is the dihedral defined by the carboxyl carbon, the anomeric carbon, the glycosidic oxygen, and the aglyconic carbon, and $\psi$ is the dihedral angle defined by the anomeric carbon, the glycosidic oxygen, the aglyconic carbon, and the aglyconic proton.

Again, ganglioside GD1a serves as a suitable illustration for detailed procedures. For ganglioside GD1a, we used 12 starting structures differing from one another by having values of the glycosidic torsion angle $\phi$ which differed from one another by 120° in an attempt to provide an adequate sampling of conformational space. All calculations were executed on either a Vaxstation 3200 or a Multiflow Trace 7 computer. A steepest descent minimizer was used for the first 400 cycles of minimization, and a conjugate gradient minimizer was used for the remainder. All minimizations were allowed to run to convergence, with convergence being defined as the RMS of the norm of the gradient as being ≤0.01 kcal/Å.

In the initial stages of our calculations with distance constraint pseudoenergies, a simplified potential surface consisting of bond, angle, and distance constraint pseudoenergy terms was used. In the next stages of our calculation, all additional torsional and nonbonded terms were added and the calculation was allowed to run to convergence. During these stages of the calculation, only constraints between protons on adjacent saccharide residues were included in the calculation. Finally, all constraints corresponding to observed connectivities in the NOESY data set were included, first in a calculation with a simplified potential surface and then in a calculation with the

[3] AMBER, copyright 1988, is obtained via a licensing agreement with the Regents of the University of California.

full potential surface. The stepwise addition of distance constraints and energy terms proved to be the most effective in avoiding local minimum traps and is analogous in some respects to the method of Braun and Gō (1986).

During the initial stages of the calculation, most distance constraints were assigned a weight corresponding to a well depth of 300 kcal/mol for a 3.0-Å constraint. Constraints involving exocyclic methylene groups or the geminal H3 protons of α-D-NeuAc residues A and B were assigned a weight corresponding to 100 kcal/mol, which reflects the greater uncertainty introduced by the fact that we did not attempt to model the rapid motional averaging and/or second-order character of the spectra which could exist for these protons.

For ganglioside GD1a 45 distance constraints were included in the calculation. Eleven of these constraints were interresidue constraints. These constraints served to define the glycosidic torsion angle $\phi$ and $\psi$ and thus the overall conformation of the oligosaccharide moiety. The remaining 34 intraresidue constraints served to define the geometry of each saccharide residue and also served as calibration standards between cross-peak intensities and interproton distances as well as restricting the geometries of exocyclic groups.

In the final stages of the calculation, a $Na^+$ counterion was placed at a distance of 2.5 Å from the carboxyl group of each α-D-NeuAc residue by using the EDIT module of the AMBER package. A distance-dependent dielectric with a slope of 1.0 was used for the calculation of electrostatic interactions. Distance constraints involving ring protons were assigned a weight corresponding to a well depth of 30 kcal for a 3.0-Å distance constraint, while distance constraints involving the geminal H3 protons of α-D-NeuAc residues A and B and exocyclic methylene groups were assigned a weight corresponding to a well depth of 15 kcal. These weights were chosen to allow for a realistic interplay of distance constraint pseudoenergies and energy terms representing the bonding and nonbonding interactions between atoms.

At this stage of the calculation on ganglioside GD1a, 44 additional constraints were added for cases where a short distance were predicted in the structures obtained upon convergence of the calculations with heavy weightings of the distance constraint pseudoenergies yet no connectivity was observed in the NOESY data set. For these additional constraints, the interproton distances were set equal to 4.0 Å, and these additional constraints were assigned the same weights as the constraints corresponding to observed connectivities. Considerable caution must be exercised in including these additional constraints as the absence of a cross-peak in a NOESY data set does not necessarily indicate that two protons are distant from one another. Other factors may also lead to the absence of cross-peaks. For instance, association between the highly charged α-D-NeuAc residues and paramagnetic contaminants could lead to systematic absences of cross-peaks. In our data, however, we found no evidence for such an association, as there were no absences of expected intraresidue connectivities in any of our data sets. In the case of GD1a, the additional constraints aided in improving structural definition and helped to better fix the orientations of exocyclic groups such as the *N*-acetyl groups of the two α-D-NeuAc residues and of β-D-GalNAc III.

## Selection and Comparison of Low-Energy Structures

To establish a preference among the structures obtained upon convergence of our molecular mechanics calculations, we have chosen to use the sum of the molecular mechanics energy and the total distance constraint pseudoenergy (Holak et al., 1988). On the one hand, significant violations of experimental distance constraints result in an increase in the total distance constraint pseudoenergy. On the other hand, satisfying experimental distance constraints by violating normal bonding geometries results in an increase in the molecular mechanics energy. Therefore, the selection of minimum energy structures on the basis of the total energy represents a reasonable means of choosing among these structures, particularly if the weightings of the distance constraint pseudoenergy terms are chosen to allow for a realistic interplay between NMR distance constraints and chemical bonding constraints.

In Table III, we present a list of $\phi$, $\psi$ values for the five lowest energy structures for ganglioside GD1a generated by the above procedure. Also in Table III, we present a breakdown of the energetic data for these low-energy structures, which we have designated 1–5, with structure **1** being the lowest energy structure and structure **5** the highest. All have similar total energies lying within 22 kcal of the apparent global minimum of −3504 kcal/mol. The total distance constraint pseudoenergies for each of these structures are similar, lying between −3328 and −3315 kcal/mol, which indicates that the magnitudes of the violations of the experimental distance constraints are all similar. The variations in the molecular mechanics energies are larger, ranging from −180 kcal/mol for structure **2** to −163 kcal/mol for structure **5**. Energy analysis, however, suggests that much of this variation is due to variations in the electrostatic contributions to the molecular mechanics energies for these structures. Electrostatic interactions are weighted heavily by the use of a distance-dependent dielectric and the presence of two highly charged α-D-NeuAc residues in these calculations, and we should be aware of a possible overemphasis of these effects. We therefore hesitate to choose among structures such as those in Table III on the basis of molecular mechanics energies alone.

To better assess the conformational differences among these low-energy structural solutions, RMS deviations between the Cartesian coordinates of the structures were computed by using the orthogonal transformation routine of the program MOULD.[4] Here, the structures were superimposed by moving the centroids of the structures to the origin and formulating a rotation matrix which superimposed the structures for minimum RMS deviation.

In Table IV, we present two types of RMS deviations for the Cartesian coordinates obtained upon comparing structures **2**–**5** to structure **1**. The first, designated $RMS_{all}$, corresponds to the deviations obtained when all atoms in the oligosaccharide moiety of GD1a were included in the comparison. These deviations ranged from 1.1 Å for structure **3** to 1.4 Å for structure **2**. The second set of deviations, designated $RMS_{main}$, corresponds to the deviations obtained when exocyclic groups, whose orientations were unconstrained by NMR distance constraints, were excluded from the comparison. These deviations were all ≤0.4 Å. Thus, these five lowest energy structures do not differ greatly in their overall conformation.

## Comparison to Structures of Gangliosides GM1 and GM1b

In Table III, we also present structural and energetic data for the six lowest energy structural solutions for gangliosides GM1 and GM1b. For both of these gangliosides, the variations in the total distance constraint pseudoenergies and in the

[4] MOULD, 1988, is a program written at Yale University by Dr. Simon K. Kearsley.

Table III: Structural Data for Gangliosides GM1, GM1b, and GD1a

| | 1 | 2 | 3 | 4 | 5 | 6 |
|---|---|---|---|---|---|---|
| GM1 | | | | | | |
| $\phi, \psi_{II,I}$ | 48, 337 | 41, 332 | 50, 336 | 40, 329 | 48, 337 | 47, 332 |
| $\phi, \psi_{III,II}$ | 26, 45 | 25, 45 | 27, 44 | 27, 45 | 25, 45 | 36, 44 |
| $\phi, \psi_{IV,III}$ | 46, 313 | 38, 314 | 30, 319 | 46, 310 | 45, 316 | 325, 342 |
| $\phi, \psi_{A,II}$ | 83, 56 | 85, 61 | 84, 58 | 80, 57 | 77, 56 | 83, 47 |
| $E_{total}$[a] | −2899 | −2898 | −2895 | −2890 | −2890 | −2890 |
| $E_{NOE}$[b] | −2821 | −2814 | −2820 | −2816 | −2820 | −2814 |
| $E_{MM}$[c] | −78 | −84 | −75 | −74 | −70 | −76 |
| GM1b | | | | | | |
| $\phi, \psi_{II,I}$ | 49, 339 | 49, 339 | 42, 342 | 36, 337 | 47, 344 | 50, 344 |
| $\phi, \psi_{III,II}$ | 351, 314 | 350, 314 | 356, 307 | 351, 315 | 5, 303 | 6, 302 |
| $\phi, \psi_{IV,III}$ | 16, 331 | 28, 331 | 5, 339 | 24, 331 | 21, 332 | 22, 330 |
| $\phi, \psi_{B,IV}$ | 28, 30 | 58, 82 | 30, 32 | 62, 78 | 38, 36 | 40, 37 |
| $E_{total}$[a] | −2742 | −2735 | −2734 | −2726 | −2723 | −2720 |
| $E_{NOE}$[b] | −2660 | −2657 | −2664 | −2658 | −2658 | −2658 |
| $E_{MM}$[c] | −82 | −78 | −70 | −68 | −65 | −62 |
| GD1a | | | | | | |
| $\phi, \psi_{II,I}$ | 49, 334 | 42, 344 | 52, 345 | 41, 343 | 41, 343 | |
| $\phi, \psi_{III,II}$ | 49, 37 | 52, 31 | 50, 37 | 51, 32 | 52, 23 | |
| $\phi, \psi_{IV,III}$ | 341, 338 | 341, 334 | 336, 341 | 329, 345 | 342, 342 | |
| $\phi, \psi_{A,II}$ | 67, 33 | 79, 37 | 77, 32 | 81, 26 | 75, 27 | |
| $\phi, \psi_{B,IV}$ | 312, 26 | 315, 49 | 313, 22 | 312, 42 | 318, 44 | |
| $E_{total}$[a] | −3504 | −3500 | −3498 | −3491 | −3482 | |
| $E_{NOE}$[b] | −3328 | −3320 | −3328 | −3315 | −3319 | |
| $E_{MM}$[c] | −176 | −180 | −170 | −176 | −163 | |

[a] Sum of molecular mechanics energy and distance constraint pseudoenergy. [b] Sum of all distance constraint pseudoenergy terms. [c] Molecular mechanics energy.

Table IV: Structural Comparison Data for Gangliosides GM1, GM1b, and GD1a

| | 2 | 3 | 4 | 5 | 6 |
|---|---|---|---|---|---|
| GM1 | | | | | |
| $RMS_{all}$[a] | 1.2 | 1.2 | 0.9 | 1.2 | 1.7 |
| $RMS_{main}$[b] | 0.3 | 0.3 | 0.3 | 0.3 | 1.0 |
| $RMS_{I-III,A}$[c] | 0.2 | 0.1 | 0.3 | 0.3 | 0.3 |
| GM1b | | | | | |
| $RMS_{all}$[a] | 2.4 | 1.3 | 2.3 | 1.3 | 1.9 |
| $RMS_{main}$[b] | 1.5 | 0.4 | 1.4 | 0.8 | 0.9 |
| $RMS_{I-IV}$[c] | 0.2 | 0.3 | 0.3 | 0.4 | 0.5 |
| GD1a | | | | | |
| $RMS_{all}$[a] | 1.4 | 1.1 | 1.3 | 1.3 | |
| $RMS_{main}$[b] | 0.4 | 0.3 | 0.3 | 0.3 | |

[a] RMS deviation computed with all atoms in oligosaccharide moiety included in comparison. [b] RMS deviation computed with exocyclic groups whose orientations were unconstrained by NMR distance constraints excluded from comparison. [c] RMS deviation computed with both unconstrained exocyclic groups and β-D-Gal IV excluded from comparison. [d] RMS deviation computed with both unconstrained exocyclic groups and α-D-NeuAc B excluded from comparison.

molecular mechanics energies were similar to the variations noted previously for ganglioside GD1a. In Table IV, we also present RMS deviations of the Cartesian coordinates which were obtained by comparing structures **2–6** to structure **1** for gangliosides GM1 and GM1b. For both of these gangliosides, we present three sets of RMS deviations. Two of these sets, which were designated $RMS_{all}$ and $RMS_{main}$, were obtained by using the same protocol as was used to calculate the corresponding RMS deviations for ganglioside GD1a. For ganglioside GM1, the values of $RMA_{all}$ ranged from 0.9 Å for structure **4** to 1.7 Å for structure **6**, while the values of $RMS_{main}$ ranged from 0.3 Å for structures **2–5** to 1.0 Å for structure **6**. For ganglioside GM1, the third set was designated $RMS_{I-III,A}$ and was obtained by excluding both unconstrained exocyclic groups and β-D-Gal IV from the comparison. Values of $RMS_{I-III,A}$ were all ≤0.3 Å. For ganglioside GM1b, the values of $RMS_{all}$ ranged from 1.3 Å for structure **3** to 2.4 Å for structure 2, while values of $RMS_{main}$ ranged from 0.4 Å for structure **3** to 1.5 Å for structure **2**. For this ganglioside, the third set of RMS deviations was designated $RMS_{I-IV}$ and was obtained by excluding both unconstrained exocyclic groups and α-D-NeuAc B from the comparison. Values of $RMS_{I-IV}$ were all ≤0.5 Å.

In Table V, we present a list of RMS deviations for the observed interresidue distance constraints for gangliosides GM1, GM1b, and GD1a. Intraresidue distance constraints, which are not included in Table V, were typically satisfied within ±0.1 Å. The largest violations of nonobserved constraints (those arbitrarily set to 4.0 Å) were typically less than −0.6Å. In Table V, we also present a list of significant deviations (deviations ≥0.5 Å) for the distance constraints corresponding to observed NOE connectivities.

In most cases, the combination of low RMS deviations and small numbers of large violations suggests that the one-state structural solutions represent a reasonable fit to data. For a few glycosidic linkages, such as the NeuAc(α2–3)Gal linkage in ganglioside GM1, our one-state structural solutions do not, however, satisfy all of the observed distance constraints. In these cases, multiple-state treatments of data (Scarsdale et al., 1988; Kim & Prestegard, 1989) are possible; however, as we have shown in our previous work (Scarsdale et al., 1988, 1990), small numbers of violations of long-range constraints can indicate minor contributions from conformers with close contacts of selected proton pairs rather than high levels of conformational flexibility.

In Figure 3, we present stereoviews of the superpositions of the low-energy structural solutions for each of the gangliosides in Figure 1. These superpositions were also computed by using the orthogonal transformation routine of MOULD. In computing these superpositions, unconstrained exocyclic groups were excluded from the comparison.

Examination of the data in Tables III–V and in Figure 3 reveals that a combination of distance constraint pseudoenergies and molecular mechanics calculations converged to a unique structural definition for many of the glycosidic linkages

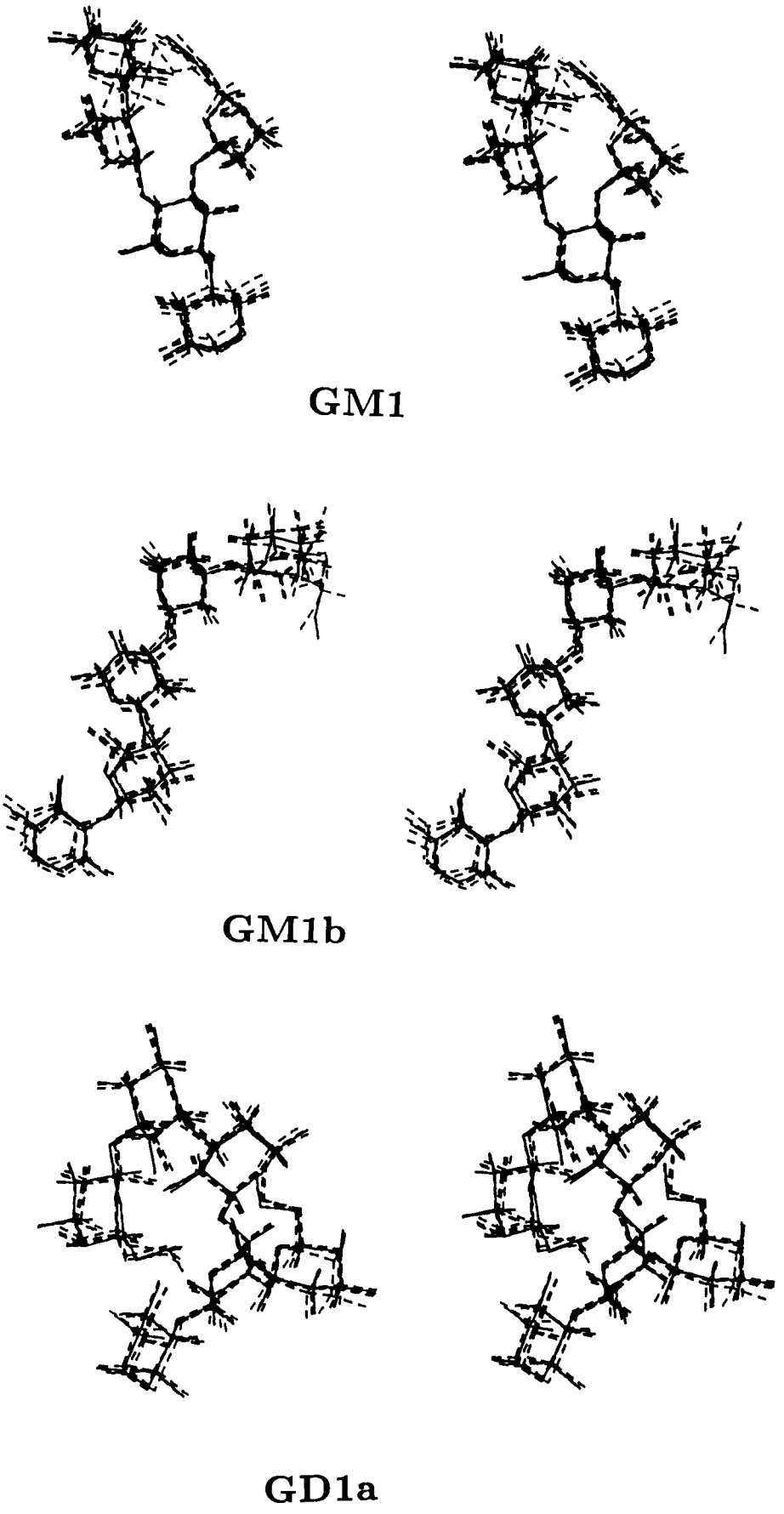


FIGURE 3: Superpositions of low-energy structural solutions for gangliosides GM1, GM1b, and GD1a. In computing these superpositions, unconstrained exocyclic groups were excluded from the comparison. For each of these superpositions, the lowest energy structural solution is designated by a solid line, while other low-energy structural solutions are denoted by dashed or by dotted lines.

Table V: Deviations from Experimental Distance Constraints for Gangliosides GM1, GM1b, and GD1a

| | 1 | 2 | 3 | 4 | 5 | 6 |
|---|---|---|---|---|---|---|
| GM1 | | | | | | |
| $RMS_{obs}$[a] | 0.16 | 0.16 | 0.16 | 0.16 | 0.16 | 0.15 |
| largest violation[b] (Å) | II(4)–A(3e) +1.6 | II(4)–A(3e) +1.6 | II(4)–A(3e) +1.6 | II(4)–A(3e) +1.6 | II(4)–A(3e) +1.6 | II(4)–A(3e) +1.5 |
| other violations ≥ 0.5 Å[b] | II(4)–III(1) +0.6 | II(4)–III(1) +0.6 II(4)–A(3a) 0.5 | II(4)–III(1) +0.6 | II(4)–III(1) +0.6 | II(4)–III(1) +0.5 | II(4)–III(1) +0.6 |
| GM1b | | | | | | |
| $RMS_{obs}$[c] | 0.09 | 0.09 | 0.08 | 0.10 | 0.08 | 0.08 |
| largest violation[b] (Å) | III(1)–II(5) +0.7 | III(1)–II(5) +0.7 | III(1)–II(5) +0.6 | III(1)–II(5) +0.7 | III(1)–II(5) +0.6 | III(1)–II(5) +0.6 |
| GD1a | | | | | | |
| $RMS_{obs}$[d] | 0.07 | 0.06 | 0.08 | 0.08 | 0.08 | |
| largest violation[b] (Å) | III(1)–II(3) +0.6 | III(1)–II(3) +0.6 | III(1)–II(3) +0.7 | III(1)–II(3) +0.7 | III(1)–II(3) +0.7 | |

[a] RMS deviation calculated for the 11 distance contraints for ganglioside GM1 which corresponded to observed interresidue connectivities. [b] For constraints corresponding to observed interresidue connectivities. [c] RMS deviation calculated for the eight distance constraints for ganglioside GM1b which corresponded to observed interresidue connectivities. [d] RMS deviation calculated for the 11 distaince constraints for ganglioside GD1a which corresponded to observed interresidue connectivities.

in gangliosides GM1, GM1b, and GD1a. In the case of ganglioside GM1, this combination has converged to essentially a single minimum for the Gal($\beta$1–4)Glc (II,I), GalNAc($\beta$1–4)Gal (III,II), and NeuAc($\alpha$2–3)Gal (A,II) linkages. For these linkages, $\phi$, $\psi$ values typically agreed within ±10°. Larger variations, however, were observed for the terminal Gal($\beta$1–3)GalNAc (IV,III) linkage, particularly for structure **6**.

In the case of ganglioside GM1b, these data suggest that many of the differences in the low-energy structural solutions correspond to differences in the orientation of the terminal $\alpha$-D-NeuAc residue. Furthermore, these data suggest the presence of two distinct sets of minimum energy structures. The first set, which includes structures **1**, **3**, **5**, and **6** has $\phi$, $\psi$ values for the terminal NeuAc($\alpha$2–3)Gal linkage which are near 30°, 30°, while the second set of structures, which includes structures **2** and **4**, has $\phi$, $\psi$ values for this linkage which are near 60°, 80°. Finally, these data suggest that although the variations in the $\phi$, $\psi$ values for the Gal($\beta$1–4)Glc (II,I) and GalNAc($\beta$1–4)Gal (III,II) linkages were somewhat larger than those typically observed for ganglioside GM1, the calculation converged to structures in which the orientations of the core oligosaccharide residues were quite similar. This was particularly true of structures **1**–**4** for which the values of $RMS_{I-IV}$ were all ≤0.3 Å.

In the case of ganglioside GD1a, these data indicate that our calculations have converged to structures which are remarkably similar in terms of the orientation of their saccharide residues. $\phi$, $\psi$ values for the Gal($\beta$1–4)Glc (II,I), GalNAc($\beta$1–4)Gal (III,II), Gal($\beta$1–3)GalNAc (IV,III), and internal NeuAc($\alpha$2–3)Gal (A,II) linkages agreed within ±14° for structures **1**–**5**. Slightly larger variations were observed in the $\psi$ values for the terminal NeuAc($\alpha$2–3)Gal (B,IV) linkage.

## Discussion

Although there is evidence for some conformational variability for each of the ganglioside structures discussed previously, we shall focus on the one or two structural solutions with the lowest total energy for each of these gangliosides. In all cases, the lowest energy structural solutions represent an excellent fit of the distance constraints corresponding to the observed connectivities, as well as having molecular mechanics energies within 6 kcal/mol of the structural solution with the lowest molecular mechanics energy. In Figure 4, we present stereoviews of these lowest energy structural solutions for gangliosides GM1, GM1b, and GD1a.

Here, we shall focus our discussion on the structural variations in two oligosaccharide substructures, the Gal($\beta$1–3)-GalNAc($\beta$1–4)Gal($\beta$1–4)Glc core oligosaccharide sequence, which is common to all of these gangliosides, and the NeuAc($\alpha$2–3)Gal($\beta$1–3)GalNAc($\beta$1–4)Gal($\beta$1–4)Glc, or GM1b oligosaccharide sequence, which is common to gangliosides GM1b and GD1a.

The three-dimensional structure of the Gal($\beta$1–3)GalNAc($\beta$1–4)Glc core oligosaccharide substructure appears to be strongly influenced by the presence of additional $\alpha$-D-NeuAc residues. Examination of the $\phi$, $\psi$ values in Table III reveals that the largest effects are at the GalNAc($\beta$1–4)Gal linkage. In Figure 5, we present a stereoview of the superposition of the core oligosaccharide sequence from gangliosides GM1, GM1b, and GD1a. In Figure 5, only the superposition of residues I and II was optimized to better depict the variations in the conformation of the III,II and IV,III glycosidic linkages among these gangliosides.

Examination of the data in Figure 5 reveals that the three-dimensional structure of the gangliotetraose core oligosaccharide sequence varies significantly among gangliosides GM1, GM1b, and GD1a. Significant deviations, relative to ganglioside GM1, were noted for ganglioside GD1a, where the presence of an additional terminal NeuAc($\alpha$2–3)Gal linkage leads to significant perturbations in the conformations of the GalNAc($\beta$1–4)Gal (III,II) and Gal($\beta$1–3)GalNAc (IV,III) linkages. The largest deviations, however, were noted for ganglioside GM1b, where the absence of an internal NeuAc($\alpha$2–3)Gal (A,II) linkage results in a conformation for the GalNAc($\beta$1–4)Gal (III,II) linkage for which the value of $\phi$ differed by −35° and the values of $\psi$ differed by −91° from the corresponding linkages for GM1.

Examination of the $\phi$, $\psi$ data in Table III for the lowest energy structures for gangliosides GM1b and GD1a reveals that the conformation of the terminal NeuAc($\alpha$2–3)Gal (B,IV) linkage is also strongly influenced by the presence of an additional NeuAc($\alpha$2–3)Gal residue. In Figure 5, we also present a stereoview of the superposition of the NeuAc($\alpha$2–3)Gal-($\beta$1–3)GalNAc($\beta$1–4)Gal($\beta$1–4)Glc oligosaccharide moiety from ganglioside GD1a and the two lowest energy structures for ganglioside GM1b. Although many of the differences between the structures of this moiety in these low-energy

Table VI: Structural Data for Energy-Refined Structures for Gangliosides GM1 and GD1a

| | native | GM1b1[a] | GM1b2[b] |
|---|---|---|---|
| GM1 | | | |
| $\phi, \psi_{II,I}$ | 59, 310 | 55, 334 | |
| $\phi, \psi_{III,II}$ | 27, 45 | 325, 335 | |
| $\phi, \psi_{IV,III}$ | 51, 304 | 50, 301 | |
| $\phi, \psi_{A,II}$ | 87, 57 | 76, 51 | |
| $E$ | −89 | −68 | |
| GD1a | | | |
| $\phi, \psi_{II,I}$ | 33, 310 | 35, 299 | 33, 301 |
| $\phi, \psi_{III,II}$ | 60, 48 | 335, 327 | 339, 324 |
| $\phi, \psi_{IV,III}$ | 341, 338 | 341, 334 | 336, 341 |
| $\phi, \psi_{A,II}$ | 65, 30 | 61, 29 | 58, 26 |
| $\phi, \psi_{B,IV}$ | 314, 24 | 326, 52 | 68, 79 |
| $E$ | −205 | −195 | −194 |

[a] Structure obtained upon refinement of structure with glycosidic torsion angles for core oligosaccharide and terminal α-D-NeuAc (for GD1a) residues set to values from structure **1** for GM1b. [b] Structure obtained upon refinement of structure with glycosidic torsion angles for core oligosaccharide and terminal α-D-NeuAc (for GD1a) residues set to values from structure **2** for GM1b.

structural solutions for gangliosides GM1b and GD1a result from differences in the gangliotetraose core oligosaccharide moiety, the conformation of the terminal NeuAc(α2–3)Gal (B,IV) linkge in ganglioside GD1a differs significantly for the conformation in either of the low-energy structural solutions for ganglioside GM1b.

In both of the above comparisons, it appears that the presence of an internally linked sialic acid has caused a folding back of some of the core to establish some additional favorable interactions. To better understand the energetic origins of these conformational changes, it is instructive to make energy calculations for GD1a and GM1 oligosaccharides in conformations in which the core oligosaccharide residues adopt glycosidic torsion angles as close as possible to those found in the two lowest energy structures for GM1b. Energy changes were calculated by carrying out molecular mechanics minimizations in the absence of distance constraints. A similar unconstrained minimization was carried out beginning with the best pseudoenergy structures for GM1 and GD1a. These sets are designated GM1b1, GM1b2, and native, respectively. Structural and energetic data are presented in Table VI. The geometries of the energy-refined structures designated native were quite similar ($\Delta\phi, \Delta\psi \approx 20°$) to the initial structures, but had molecular mechanics energies 10–20 kcal/mol lower. For both gangliosides GM1 and GD1a, the structures that began with glycosidic torsion angles similar to GM1b showed larger changes during minimization, but maintained characteristics of the GM1b structures, particularly at the (III,II) linkage. These new structures show significantly higher energies than the native structures for GM1 and GD1a (10–20 kcal/mol).

To isolate the sources of energetic stabilization for these native structures, we have used the ANALYSIS module of AMBER to decompose the nonbonded energies for these energy-refined structures for gangliosides GM1 and GD1a on the basis of interactions between pairs of saccharide residues. In Table VII, we present a list of these pairwise interaction energies for saccharide residues not directly bonded to one another.

Table VII reveals that a prominent source of energetic stabilization for the native structure of GM1 is due to interactions between β-D-GalNAc III and α-D-NeuAc A. For the structure that is similar to the native structure, the total energy due to interactions between these two residues is −17 kcal/mol, while in the structure in which the conformation of the core oligosaccharide is similar to that of GM1b, the interaction energy was −10 kcal/mol. Further stabilization of the native structure is provided by interactions between the terminal β-D-Gal residue and α-D-NeuAc A.

To further isolate the sources of energetic stabilization, we have extended the decomposition of energies to the atomic level. In Table VIII, we present a list of pairwise interaction energies ≥10 kcal/mol between atoms on saccharide residues not directly bonded to one another. The data suggest that a prominent source of stabilization for the native structure of GM1 is due to interactions between the carboxyl group of α-D-NeuAc A and the *N*-acetyl group of β-D-GalNAc III. These interactions include a hydrogen bond between the amide

Table VII: Interaction Energies for Pairs of Saccharide Residues Not Directly Bonded to One Another for Gangliosides GM1 and GD1a

| | native | GM1b1[a] | GM1b2[b] |
|---|---|---|---|
| GM1 | | | |
| I,III | −1.4 | −0.4 | |
| I,IV | −0.5 | −0.4 | |
| I,A | 2.4 | 2.7 | |
| II,IV | −1.7 | −1.8 | |
| III,A | −16.6 | −9.7 | |
| IV,A | −2.6 | 0.1 | |
| GD1a | | | |
| I,III | −1.7 | −0.8 | −0.8 |
| I,IV | 0.0 | −0.1 | −0.1 |
| I,A | 2.2 | 2.0 | 2.0 |
| I,B | −0.3 | 0.1 | 0.8 |
| II,IV | −0.4 | −0.6 | −0.9 |
| II,B | −4.7 | 0.3 | 2.9 |
| III,A | −3.8 | −7.6 | −5.2 |
| IV,A | −1.8 | −0.1 | 0.1 |
| A,B | −54.4 | −4.2 | −1.1 |

[a] Structure obtained upon refinement in the absence of distance constraint pseudoenergies with values of glycosidic torsion angles set to values from structure **1** for GM1b. [b] Structure obtained upon refinement in the absence of distance constraint pseudoenergies with values of glycosidic torsion angles set to values from structure **2** for GM1b.

Table VIII: Interaction Energies ≥10 kcal/mol between Pairs of Atoms on Saccharide Residues Not Directly Bonded to One Another for Gangliosides GM1 and GD1a

| | native | GM1b1[a] | GM1b2[b] |
|---|---|---|---|
| GM1 | | | |
| III(N2)–A(O1a) | 21.6 | 4.5 | |
| III(HN)–A(O1a) | −25.8 | −5.7 | |
| III(C7)–A(O1a) | −18.0 | [c] | |
| III(O7)–A(HO7) | [c] | −10.4 | |
| III(O7)–A(O7) | [c] | 12.2 | |
| GD1a | | | |
| A(O1a)–B(O8) | 24.6 | [c] | [c] |
| A(O1a)–B(HO8) | −33.6 | [c] | [c] |
| A(O1a)–B(O9) | 25.1 | [c] | [c] |
| A(O1a)–B(HO9) | −33.3 | [c] | [c] |
| A(O8)–B(O1b) | 13.5 | 3.6 | [c] |
| A(O9)–B(O1b) | 23.7 | [c] | [c] |
| A(HO9)–B(O1b) | −33.8 | [c] | [c] |
| A(O8)–B(O8) | 12.9 | 12.5 | [c] |
| A(HO8)–B(O8) | −16.7 | −15.3 | [c] |
| A(O7)–III(O7) | [c] | 12.0 | 13.3 |
| A(HO7)–III(O7) | [c] | −15.1 | −15.2 |
| III(C7)–B(O1a) | [c] | [c] | −10.5 |
| III(O7)–B(O1a) | [c] | [c] | 10.8 |

[a] Structure obtained upon refinement in the absence of distance constraint pseudoenergies with values of glycosidic torsion angles set to values from structure **1** for GM1b. [b] Structure obtained upon refinement in the absence of distance constraint pseudoenergies with values of glycosidic torsion angles set to values from structure **2** for GM1b. [c] Interaction energy between these two atoms was less than 3.0 kcal/mol in this structure and therefore was not a significant source of stabilization/destabilization.

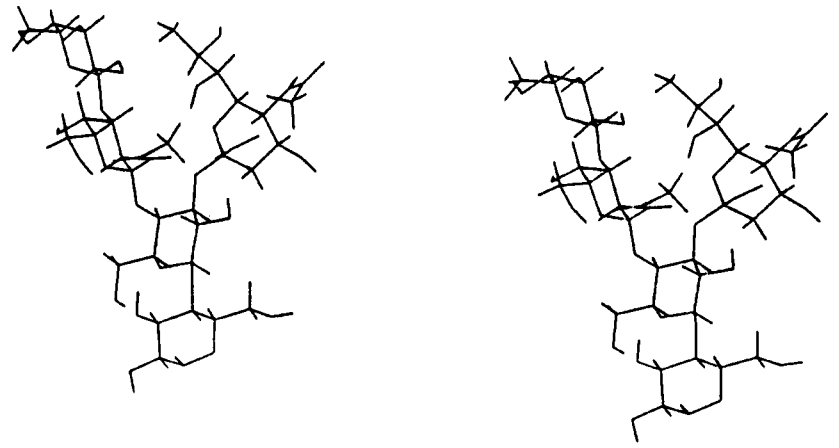

GM1

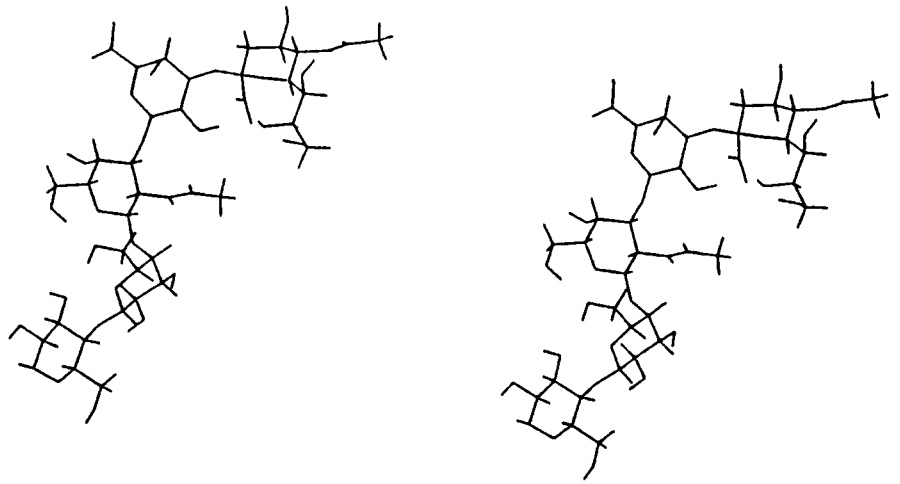

GM1b

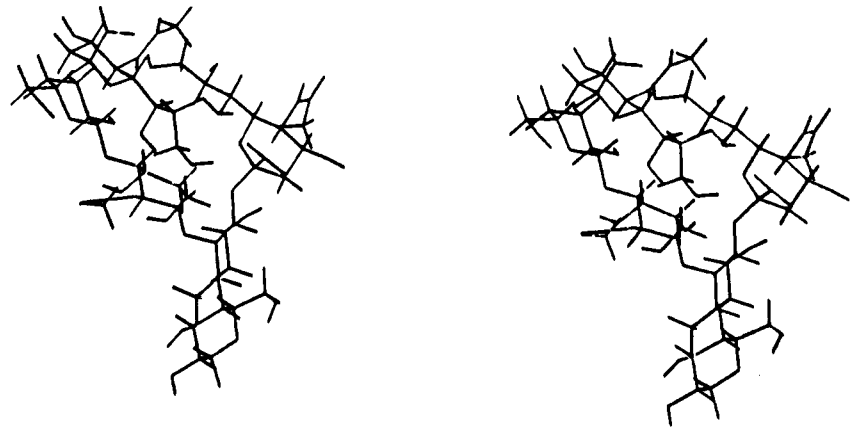

GD1a

FIGURE 4: Stereoviews of lowest energy structural solutions for gangliosides GM1, GM1b, and GD1a.

proton of β-D-GalNAc III and one of the oxygens of the $COO^-$ group of the α-D-NeuAc residue as well as electrostatic interactions between the carbonyl carbon of the *N*-acetyl group and of β-D-GalNAc III and the oxygens of the $COO^-$ group of α-D-NeuAc A. In other words, the perturbations observed in the glycosidic torsion angles for the oligosaccharide moiety

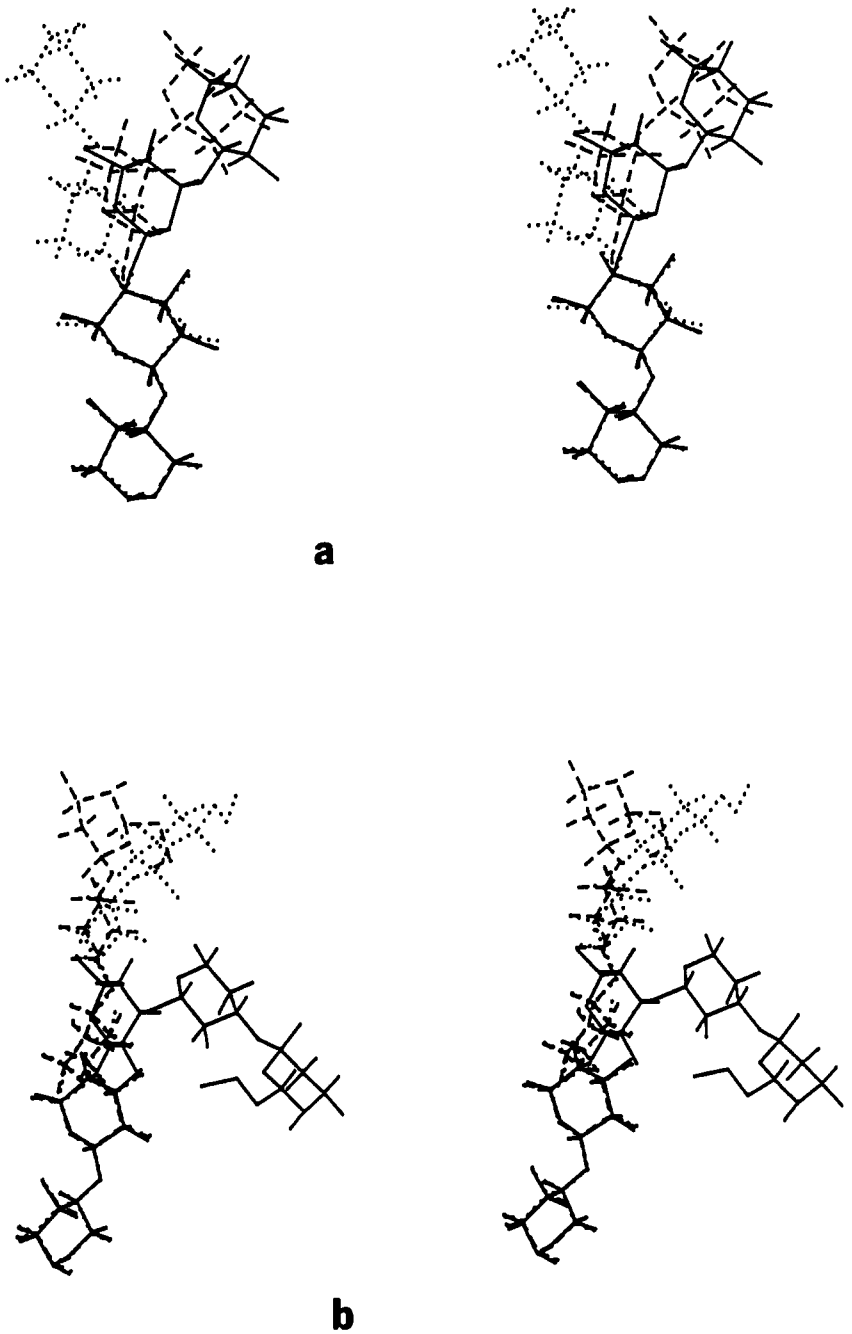


FIGURE 5: Stereoviews of superimposed oligosaccharide structures. (a) Core oligosaccharide moiety from lowest energy structural solutions for GM1 (—), GM1b (···), and GD1a (---). (b) GM1b oligosaccharide moiety from structures **1** (---) and **2** (···) for ganglioside GM1b and structure **1** for ganglioside GD1a (—). In computing these superpositions, only atoms from residues I and II were included in the calculation to emphasize structural differences in the conformation of the more terminal linkages.

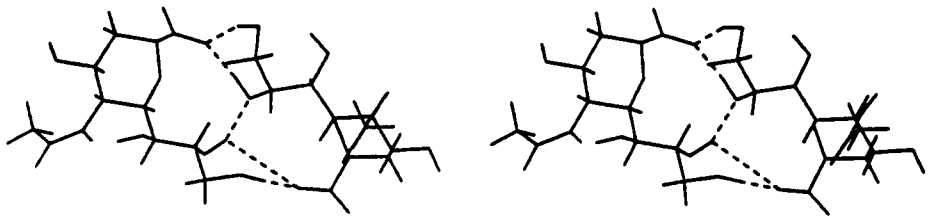

FIGURE 6: Stereoview of the hydrogen-bonding network between the two α-D-NeuAc residues in ganglioside GD1a. Hydrogen bonds A(O1a)–B(HO8), A(O1a)–B(HO9), A(HO8)–B(O1b), A(HO9)–B(O1b), and A(HO8)–B(O8) are shown.

of ganglioside GM1 appear to result from attractive interactions between specific pairs of saccharide residues, most notably β-D-GalNAc III and α-D-NeuAc A. This observation is consistent with suggestions made previously on the basis of a more qualitative analysis (Koerner et al., 1983; Sillerud & Yu, 1983).

The glycosidic torsion angles for the lowest energy one-state structural solutions for ganglioside GD1a differ significantly from the corresponding dihedrals in the lowest energy structural solutions for ganglioside GM1. It therefore seems likely that these structural perturbations result from a different set of interactions than those responsible for the perturbations in

ganglioside GM1. Examination of the data in Table VII reveals that this is the case. These data indicate that the primary source of stabilization for the native structure of GD1a is due to interactions between the two α-D-NeuAc residues. In the energy-refined structure with glycosidic torsion angles which were similar to the native structure, this interaction energy was −54 kcal/mol, while in the structures in which glycosidic torsion angles began at those observed for the core oligosaccharide moiety and terminal NeuAc(α2–3)Gal linkage in GM1b, it is only −4 and −1 kcal/mol, respectively.

The data in Table VIII suggest that a prominent source of stabilization for the native GD1a structure is the presence of a rather extensive hydrogen-bonding network between the two α-D-NeuAc residues. This network consists of hydrogen bonds between the carboxyl group of α-D-NeuAc A and the glyceryl side chain of α-D-NeuAc B, the glyceryl side chain of α-D-NeuAc A, and the carboxyl group of α-D-NeuAc B, as well as hydrogen bonds btween the two glyceryl side chains. In Figure 6, we present a stereoview of the hydrogen-bonding network from the native structure of ganglioside GD1a.

## Conclusion

We have shown that the presence of α-D-NeuAc residue in an oligosaccharide sequence can have significant and far-reaching structural consequences. Gangliosides that differ in the linkage site for a single α-D-NeuAc residue can have three-dimensional structures of common oligosaccharide sequences which are strikingly different, as is observed on comparing the three-dimensional structure of the Gal(β1–3)-GalNAc(β1–4)Gal(β1–4)Glc core oligosaccharide sequence in gangliosides GM1 and GM1b. The addition of a second α-D-NeuAc residue seems to further amplify these effects. For instance, in the case of ganglioside GD1a, the addition of a terminal NeuAc(α2–3)Gal linkage to the GM1 oligosaccharide structure resulted in significant perturbations to the glycosidic torsion angles for the Gal(β1–3)GalNAc (IV,III), GalNAc(β1–4)Gal (III,II), and NeuAc(α2–3)Gal (A,II) linkages as compared to the corresponding dihedrals in ganglioside GM1.

Furthermore, we believe these structural perturbations are the result of through-space interactions involving specific pairs of saccharide residues. For instance, the structural perturbations in ganglioside GM1 appear to be energetically stabilized by hydrogen-bonding interactions between β-D-GalNAc III and α-D-NeuAc A. In the case of ganglioside GD1a structural perturbations appear to be energetically stabilized by the presence of a rather extensive hydrogen-bonding network between the two α-D-NeuAc residues.

Again, we remind the reader that these structures are not necessarily similar to the in vivo conformations which are important for the biological functions of these gangliosides. The choice of solvent in this investigation is nonphysiological. In fact, given the prominent role played by intramolecular hydrogen-bonding interactions as sources of energetic stabilization for the ganglioside structures determined in DMSO, the structures for these gangliosides may be significantly different in aqueous solvent. DMSO is an excellent hydrogen-bond acceptor, but not a hydrogen-bond donor. We have demonstrated, however, that intramolecular interactions such as those postulated above can induce changes in core oligosaccharide conformation and may, in fact, be responsible for some observed variations in receptor affinities among oligosaccharides with closely related primary structures.

## Acknowledgments

We thank Dr. T. Ariga for the generous gift of GM1b. We thank Peter C. Demou for his expert technical assistance with the instrumental aspects of this work.

**Registry No.** GM1, 104443-62-1; GM1b, 57576-20-2; GD1a, 104443-59-6.

## References

Ando, S., & Yu, R. K. (1977) *J. Biol. Chem. 252*, 6247–6250.
Ariga, T., & Yu, R. K. (1987) *J. Lipid Res. 28*, 285–291.
Braun, W., & Gō, N. (1986) *J. Mol. Biol. 186*, 611–626.
Breg, J., Kroon-Batenburg, L. M. J., Strecker, G., Montreuil, J., & Vliegenthart, J. F. G. (1989) *Eur. J. Biochem. 178*, 727–739.
Holak, T. A., Foreman, J. A., & Prestegard, J. H. (1987a) *Biochemistry 26*, 4152–4160.
Holak, T. A., Scarsdale, J. N., & Prestegard, J. H. (1987b) *J. Magn. Reson. 74*, 564–569.
Holak, T. A., Kearsley, S. K., Kim, Y., & Prestegard, J. H. (1988) *Biochemistry 27*, 6135–6142.
Homans, S. W., Dwek, R. A., Boyd, J., Mahmoudin, M., Richards, W. G., & Rademacher, T. W. (1986) *Biochemistry 25*, 6342–6350.
Jennings, H. J., & Kasper, D. L. (1981) *Biochemistry 20*, 4518–4522.
Jennings, H. J., Rossel, D. C., & Kasper, D. L. (1980) *Can. J. Biochem. 58*, 112–120.
Kasper, D. L., Baker, C. J., Baltimore, R. S., Crabb, J. H., Schiffman, G., & Jennings, H. J. (1979) *J. Exp. Med. 149*, 327–329.
Koerner, T. A. W., Prestegard, J. H., Yu, R. K., & Demou, P. C. (1983) *Biochemistry 22*, 2676–2686.
Lemieux, R. U., Bock, K., Delbaer, L. T. J., Koto, S., & Rao, V. S. (1980) *Can. J. Chem. 58*, 631–652.
Sabesean, S., Bock, K., & Lemieux, R. U. (1984) *Can. J. Chem. 62*, 1034–1045.
Scarsdale, J. N., Prestegard, J. H., Ando, T., Hori, T., & Yu, R. K. (1986a) *J. Carbohydr. Res. 155*, 45–56.
Scarsdale, J. N., Yu, R. K., & Prestegard, J. H. (1986b) *J. Am. Chem. Soc. 108*, 6778–6784.
Scarsdale, J. N., Ram. P., Prestegard, J. H., & Yu, R. K. (1988) *J. Comput. Chem. 9*, 133–147.
Scarsdale, J. N., Ram. P., Prestegard, J. H., & Yu, R. K. (1990) *Computer Modeling of Carbohydrates* (French, A., & Brady, R. O., Eds.) ACS Symposium Series 430, pp 240–266, American Chemical Society, Washington, DC.
Schifferle, R. E., Jennings, H. J., Wessell, M. R., Katzellenbogen, E., Roy, R., & Kasper, D. L. (1985) *J. Immunol. 135*, 4164–4170.
Sillerud, L. O., & Yu, R. K. (1983) *Carbohydr. Res. 113*, 173–188.
States, D. J., Haberkorn, R. A., & Reuben, D. J. (1982) *J. Magn. Reson. 48*, 286–292.
Thørgeson, H., Lemieux, R. U., Bock, K., & Meyer, B. (1982) *Can. J. Chem. 60*, 44–57.
Weiner, P. K., & Kollman, P. A. (1981) *J. Comput. Chem. 2*, 287–303.